Proceedings of the International Conference on Heat Exchanger Fouling and Cleaning - 2024 (Peer-reviewed)
April 21–26, 2024, Lisbon, Portugal; Editors: H.U. Zettler and E.M. Ishiyama

A CLEANING MODEL FOR FILM-LIKE SOILS WITH TRANSITION BETWEEN CLEANING MECHANISMS

***C. Golla[1], V. Liebmann[1], S. Jena[1], J. Fröhlich[1], F. Rüdiger[1] and H. Köhler[2]**

[1] Institute of Fluid Mechanics, Technische Universität Dresden, Germany, christian.golla@tu-dresden.de

[2] Institute of Natural Materials Technology, Technische Universität Dresden, Germany

ABSTRACT

Optimizing the cleaning time of thin fouling layers, termed *soil*, is an omnipresent challenge in the food processing industry. One approach to address this problem is to identify different prototypical modes of soil removal, called *cleaning mechanisms*, and to simulate the cleaning process with a dedicated model for each cleaning mechanism. Realistic cleaning procedures, however, involve chemicals and varying operating conditions that cause the cleaning mechanism to change. In the present paper, a cleaning model combining different cleaning mechanisms is presented. The model transits inherently between the different cleaning mechanisms and accounts for the most important influencing factors on cleaning, like flow velocity, hydroxide ion concentration, and temperature. Each model component is validated using both experimental and numerical data. Finally, in a case study, the cleaning of a proteinaceous soil in a heat exchanger is investigated, where a simplified cleaning-in-place procedure is optimized using the new model.

INTRODUCTION

A universal and economically viable method to avoid fouling has not yet been developed [1]. Hence, cleaning surfaces is an essential operation in industrial and environmental applications [2]. Cleaning causes high ecological and economic costs [3] due to the consumption of energy, chemicals, and water [4]. Furthermore, in the food processing industry, insufficient cleaning results in a high risk for cross-contamination [5]. To avoid problems resulting from insufficient cleaning, high safety factors are introduced and overdimensioning is accepted [6]. Many experts in the field of fouling and cleaning state that there is huge potential for optimization of cleaning processes, which can only be used if the physical and chemical mechanisms involved in cleaning processes are better understood [7–11]. A possibility to assess this optimization potential is a successive investigation of the relevant effects on cleaning and the inclusion of this understanding into models [10]. Once these models are available, cleaning procedures can be simulated under various operating conditions, and the results can be used to find optimal parameters [11].

The present authors' focus on developing models for thin, film-like fouling layers, termed *soil*. The ansatz pursued is the *boundary condition cleaning model* (BCCM) approach, first introduced in [12]. In a BCCM, the computation of the flow is decoupled from the calculation of the soil removal. This decoupling is valid if the following assumptions are fulfilled [11, 13, 14]: 1. The soil height is negligible compared to the characteristic dimensions of the flow. 2. There is no influence of the cleaning progress on the fluid forces acting on the soil. Another assumption, which is not necessary for decoupling, is that the soil height is negligible compared to the remaining soil dimensions, i.e., in the tangential direction. This allows modeling of transport processes into the soil, like swelling and heating, by one-dimensional transport equations, which results in lower computational costs.

The way the removal of the soil is modeled depends on the soils response when subjected to a certain cleaning procedure. This mode of removal is termed *cleaning mechanism* [15]. The cleaning mechanisms used in the BCCM framework, according to Köhler et al. [16], are *diffusive dissolution* [12, 17, 18], *cohesive separation* [13], *adhesive detachment* [11, 19], and *viscous shifting* [14], as illustrated in Fig. 1. In case of diffusive dissolution, soil molecules are transported into the cleaning fluid by diffusion. Cohesive separation occurs if the hydrodynamic loads acting on the soil overcome the cohesion within the soil, causing soil chunks to be removed. If the adhesion between soil and substrate is weaker than the cohesion within the soil, the loads acting on the soil cause adhesive detachment, whereby large patches of the soil are removed at once. Viscous shifting is present if the

ISBN: 978-0-9984188-3-4; Published online www.heatexchanger-fouling.com

applied loads cause the soil to flow, often accompanied by interfacial instabilities.

Diffusive dissolution differs fundamentally from the other three cleaning mechanisms. With diffusive dissolution, removal is achieved by a diffusion mechanism, whereas with all other cleaning mechanisms, removal is achieved by a mechanical load. The diffusive mass flux of soil into the cleaning fluid is typically modeled based on the wall-normal gradient of the soil concentration [12, 20]. Hence, diffusive dissolution requires knowledge of species transport in the cleaning fluid, which is typically achieved by solving a convection-diffusion equation. In the models for the three other cleaning mechanisms, the mechanical load relevant for soil removal is extracted from the flow computation, and thus no additional transport equation needs to be solved.

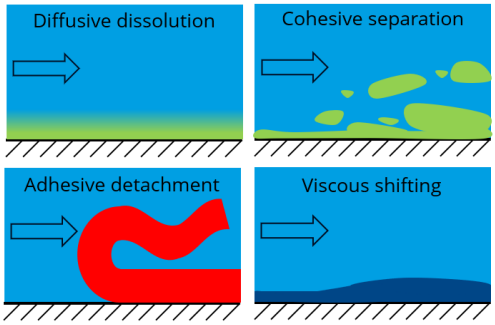

Fig. 1. Cleaning mechanisms defined by Köhler et al. [16], figure after [18].

Currently, a BCCM for each cleaning mechanism is available [11–14, 17–19]. The BCCMs available were developed using water at room temperature as cleaning fluid so far. According to Sinners circle [6], however, temperature and chemical composition of the cleaning fluid, mechanical stress applied to the soil, and the operating time are the most important influencing factors for cleaning of soils. The BCCMs available account for mechanical stress applied to the soil and time effects. However, the influencing factors temperature and chemical composition of the cleaning fluid are missing thus far.

A large body of literature is available reporting the effects of temperature and sodium hydroxide concentration of the cleaning fluid. Sodium hydroxide is the most widely used chemical in cleaning. In a review provided by Goode et al. [1], these effects and many others were studied in detail, which is summarized. Goode et al. [1] follow the classification of soils suggested by Fryer and Asteriadou [21] according to their cleanability. Type 1 soils can be cleaned entirely using hot water only. In various studies [22–24] with type 1 soils, like tomato paste, shampoo, and toothpaste, it was found that an increase in temperature decreases the cleaning time. Type 2 soils comprise microbes and biofilms. Again, an increase in temperature causes a decrease in cleaning time [25, 26]. Finally, type 3 soils require a chemical agent to be cleaned. An example particularly relevant for the dairy industry is whey protein concentrate (WPC) or isolate (WPI), which forms on heat exchanger (HEX) surfaces during pasteurization or ultra-heat treatment. The first step in cleaning proteinaceous soils like WPC is always contact with an alkaline solution [7, 9, 10, 20, 27, 28]. Upon contact with hydroxide ions the protein matrix changes from a dense platelet structure to a hollow matrix which is swellable [29]. This allows the cleaning fluid to diffuse into the soil, causing cracks in the structure and reducing the binding forces. Many authors found that there exists an optimal hydroxide ion concentration of 0.5%(w/w) to promote this swelling process [7, 8, 29, 30]. Further increase beyond this concentration leads to polymerization of the protein, resulting in a rubber-like structure that inhibits further swelling [8, 29]. For type 3 soils, in most studies, it was found that an increase in temperature decreases the cleaning time [20, 22, 29, 31, 32], although sporadically contrary observations were made [32]. The decrease in cleaning time is attributed to an increase in diffusion speed, improved solubility, and faster protein disentanglement [27, 29, 31]. Throughout most of the studies discussed here, temperatures up to 70 °C were investigated. Applying chemicals at higher temperatures could damage facilities and cause unwanted reactions of proteins in the deposit [29]. Besides the impact on cleaning time, it was also observed that hydroxide ion concentration and temperature directly affect the cleaning mechanism [15, 33–36].

To summarize, it can be said that both, the temperature and chemical composition of the cleaning fluid markedly alter the cleaning qualitatively and quantitatively. Thus, a cleaning model that includes temperature and hydroxide ion concentration in the cleaning fluid must also include a transition between different cleaning mechanisms. In the present paper, a *combined cleaning model* for cohesive separation, adhesive detachment and viscous shifting is presented that meets this requirement. Diffusive dissolution is not considered as the main challenge here is the estimation of the wall-normal gradient of the soil concentration in the cleaning fluid via the solution of a convection-diffusion equation. In the present work, however, the focus is on developing the cleaning model itself. The model includes a new formulation of a swelling model that is able to account for the transport of water, hydroxide ions, and heat into the soil. After devising the combined cleaning model, it is validated quantitatively with pertinent reference data. Finally, the model is used to simulate a cleaning-in-place (CIP) procedure of a type 3 deposit in a HEX.

ISBN: 978-0-9984188-3-4; Published online www.heatexchanger-fouling.com

COMBINED CLEANING MODEL

Overview

The three cleaning mechanisms, cohesive separation, adhesive detachment, and viscous shifting are combined into one model. While cohesive separation and adhesive detachment can cause a removal of soil, viscous shifting only causes a redistribution, i.e. the soil is pushed out of a region of interest over time. In the previous models for cohesive separation [13] and adhesive detachment [11, 19], the soil was discretized in wall-normal direction only. In the model for viscous shifting the soil was discretized in the main flow direction into so-called segments, and mass or enthalpy fluxes between the segments were defined [14].

To combine both approaches while keeping the computational effort reasonable, the soil is discretized in the main flow direction into N_{seg} segments. Each segment i is discretized in $N_{y,i}$ cells in wall normal direction. In each segment, one-dimensional transport problems in wall normal direction are solved for the water and the hydroxide ions being transported into the soil. The heat transfer problem is solved accordingly. The discretization is illustrated in Fig. 2. The present model is formulated for a two-dimensional scenario, which is present in many cases of interest. An extension towards three-dimensional problems is possible, as already demonstrated in case of the model for adhesive detachment [19].

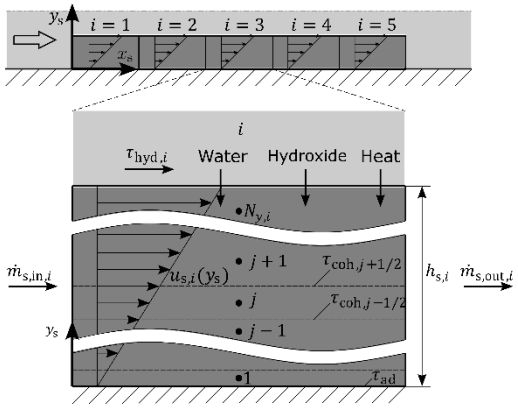

Fig. 2. Model overview. Discretization of soil into $N_{\mathrm{seg}} = 5$ segments and segments into cells.

Load calculation

The cleaning model requires the mechanical load acting on the soil as an input. The stress exerted by the flow is obtained from the CFD and is then imposed in the simulation of the soil. This amounts to one-way coupling between fluid and soil and is visualized in Fig. 3. The single-phase flow calculation uses the global coordinates x and y and provides the stress on the soil, without resolving its geometry. The evolution of the soil is simulated separately, accounting for the actual dimensions of the soil. It uses its own coordinates, x_s-y_s, with y_s resolving the thickness of the soil.

A single-phase flow solution, in particular the shear stress, can be obtained in different ways, by experimental measurements, by CFD simulations, or analytical solutions, if available. In a general flow situation, the load on the soil is constituted by a combination of pressure and shear force. In the present approach this is limited to shear forces since the height of the soil is assumed to be small, so that the side areas where the pressure force could attack are very small and, hence, negligible compared to the shear forces acting on the top surface of the soil. It is understood that scenarios exist in which pressure forces become relevant even in the case of film-like soils. Examples involve pressure oscillation or cavitation used for cleaning in some processes, but these situations are not considered here. In the present work a scalar reference value τ_{hyd} characterizing the magnitude of the load is employed. It is determined by integrating the fluid forces along the interface between the fluid and the soil, termed A_{int} here, to give

$$\tau_{\mathrm{hyd}} = \frac{1}{A_{\mathrm{int}}} \int_{A_{\mathrm{int}}} \left\| \underline{\underline{\tau}} \cdot \underline{n} \right\| \mathrm{d}A. \qquad (1)$$

All quantities in Eq. (1) are depicted in Fig. 3. The magnitude is used so that shear stresses in opposing directions do not compensate each other during the integration across the interfacial area. In cases where pressure forces are relevant, these must be included in the calculation of the reference load.

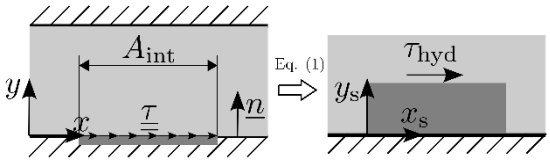

Fig. 3. Illustration of the one-way coupling for the load calculation.

Modeling of transport processes into the soil

Diffusion of water. For the modeling of the swelling process a volume of soil $V_s(t)$ is considered. Throughout the section, temporal dependencies are dropped in the notation. The mass m_s of the volume V_s can be stated as

$$m_s = m_f + m_d, \qquad (2)$$

where m_f is the mass of water within the soil layer and m_d is the dry mass of the soil, without any water. It is assumed that the swelling process only affects the water mass. Hence, m_d remains unchanged. The modeling is carried out using a Lagrangian framework, where the volume V_s always refers to the same dry mass. Furthermore, the two materials water and dry soil, are incompressible with

ISBN: 978-0-9984188-3-4; Published online www.heatexchanger-fouling.com

the densities ρ_f and ρ_d, respectively. Assuming the whole volume V_s is filled with either water or dry soil, the volume can be decomposed as

$$V_\mathrm{s} = V_\mathrm{f} + V_\mathrm{d}. \tag{3}$$

A conservation equation for the water mass in a segment can be stated as

$$\frac{\mathrm{d}m_\mathrm{f}}{\mathrm{d}t} = \frac{\mathrm{d}}{\mathrm{d}t}\int_{V_\mathrm{s}} \beta_\mathrm{f}\,\mathrm{d}V = -\int_{A_\mathrm{s}} \underline{J}_\mathrm{f,diff}\cdot\underline{n}\,\mathrm{d}A, \tag{4}$$

where β_f is the water concentration with the dimensions $\mathrm{kg/m^3}$, $A_\mathrm{s} = \partial V_\mathrm{s}$ are the bounds of the segment, $\underline{n}$ is the outward facing surface normal vector, and $\underline{J}_\mathrm{f,diff}$ are the diffusive fluxes. The diffusive fluxes are computed using Fick's law [37] of diffusion

$$\underline{J}_\mathrm{f,diff} = -D_\mathrm{f}\nabla\beta_\mathrm{f}. \tag{5}$$

Here, D_f is the apparent diffusion coefficient of the fluid. For the following discussion, an exemplary segment is considered, and the index i is dropped for convenience. The mass balance provided in Eq. (4) is applied to each cell j and only one-dimensional transport in wall-normal direction is considered, as discussed in the previous sections. The right-hand-side of Eq. (4) is discretized using the midpoint rule and the temporal derivative is discretized using the Euler-forward method, yielding

$$\frac{m''^{(n+1)}_{\mathrm{f},j} - m''^{(n)}_{\mathrm{f},j}}{\Delta t} = -J^{(n)}_{\mathrm{f,diff},j+1/2} + J^{(n)}_{\mathrm{f,diff},j-1/2}, \tag{6}$$

where the mass flux $m''^{(n)}_{\mathrm{f},j} = m^{(n)}_{\mathrm{f},j}/A_\mathrm{p}$, with A_p being the area covered by the soil. The superscript n indicates the time step and $J^{(n)}_{\mathrm{f,diff},j+1/2} = \left(\underline{J}_\mathrm{f,diff}\cdot\underline{n}\right)^{(n)}_{j+1/2}$. The fluxes are further approximated using linear interpolation

$$J^{(n)}_{\mathrm{f},j+1/2} = -D^{(n)}_{\mathrm{f},j+1/2}\left.\frac{\partial\beta_\mathrm{f}}{\partial y_\mathrm{s}}\right|^{(n)}_{j+1/2} \approx -\frac{h^{(n)}_{\mathrm{s},j+1}D^{(n)}_{\mathrm{f},j} + h^{(n)}_{\mathrm{s},j}D^{(n)}_{\mathrm{f},j+1}}{h^{(n)}_{\mathrm{s},j+1}+h^{(n)}_{\mathrm{s},j}}\frac{\beta^{(n)}_{\mathrm{f},j+1}-\beta^{(n)}_{\mathrm{f},j}}{1/2\left(h^{(n)}_{\mathrm{s},j+1}+h^{(n)}_{\mathrm{s},j}\right)}. \tag{7}$$

Herein, $h^{(n)}_{\mathrm{s},j}$ are the cell heights. Further, a relationship between soil mass, cell height and water concentration is given by

$$\beta^{(n)}_{\mathrm{f},j} = \frac{m''^{(n)}_{\mathrm{f},j}}{h^{(n)}_{\mathrm{s},j}}. \tag{8}$$

Dividing Eq. (3) by A_int yields

$$h^{(n)}_{\mathrm{s},j} = h^{(n)}_{\mathrm{f},j} + h^{(0)}_{\mathrm{d},j} = \frac{m''^{(n)}_{\mathrm{f},j}}{\rho_\mathrm{f}} + \frac{m''^{(0)}_{\mathrm{d},j}}{\rho_\mathrm{d}} \tag{9}$$

As discussed in the introduction, diffusion of cleaning fluid may be enhanced or inhibited depending on the concentration of hydroxide ions β_{OH^-}. The water concentration β_f and the temperature ϑ_s of the soil may further influence the diffusion process. Therefore, the apparent diffusion coefficient D_f is in general not constant but rather a function of the influencing factors of the form

$$D_\mathrm{f} = f(\beta_\mathrm{f}, \beta_{\mathrm{OH}^-}, \vartheta_\mathrm{s}). \tag{10}$$

To perform a simulation, the densities ρ_f, ρ_d and the relation for the diffusion coefficient Eq. (10) must be known. The initial state of the problem must be given so that the initial height $h^{(0)}_{\mathrm{s},j}$ and the initial soil mass coverage $m''_{\mathrm{s},0}$ can be computed. Furthermore, the initial and boundary conditions of the concentration are given as $\beta_\mathrm{f}(y_\mathrm{s}, t=0) = \beta_0$, $\left.\frac{\partial\beta_\mathrm{f}}{\partial y_\mathrm{s}}\right|_{y_\mathrm{s}=0} = 0$, $\beta_\mathrm{f}(y_\mathrm{s}=h_\mathrm{s}, t>0) = \beta_\mathrm{max}$. The experiments to determine these boundary conditions are described in [11].

Table 1. Conservative quantities, modelled by Eq. (11) with corresponding fluxes, boundary conditions and initial conditions. Heat capacity is represented by c_p and $\vartheta_{\mathrm{s,ref}} = 0$ °C is used as reference for the enthalpy.

Φ	φ	$\underline{J}_\mathrm{conv}$	$\underline{J}_\mathrm{diff}$	$y_\mathrm{s}=0$	$y_\mathrm{s}=h_\mathrm{s}$	$t=0$
m_f	β_f	0	$-D_\mathrm{f}\nabla\beta_\mathrm{f}$	$\frac{\partial\beta_\mathrm{f}}{\partial y_\mathrm{s}}=0$	$\beta_\mathrm{f}=\beta_\mathrm{max}$	$\beta_\mathrm{f}=c_0$
m_{OH^-}	β_{OH^-}	$\underline{u}\,\beta_{\mathrm{OH}^-}$	$-D_{\mathrm{OH}^-}\nabla\beta_{\mathrm{OH}^-}$	$\frac{\partial\beta_{\mathrm{OH}^-}}{\partial y_\mathrm{s}}=0$	$\beta_{\mathrm{OH}^-}=\beta_{\mathrm{b,OH}^-}$	$\beta_{\mathrm{OH}^-}=0$
m_d	β_d	0	0	–	–	–
H_s	$\beta_\mathrm{f}c_{p,\mathrm{f}}\vartheta_\mathrm{s}+\beta_\mathrm{d}c_{p,\mathrm{d}}\vartheta_\mathrm{s}$	$\underline{u}\,\beta_\mathrm{f}\,c_{p,\mathrm{f}}$	$-\kappa_\mathrm{s}\nabla\vartheta_\mathrm{s}$	$\vartheta_\mathrm{s}=\vartheta_\mathrm{w}$, $\kappa_\mathrm{s}\frac{\partial\vartheta_\mathrm{s}}{\partial y_\mathrm{s}}=\kappa_\mathrm{w}\frac{\partial\vartheta_\mathrm{w}}{\partial y_\mathrm{s}}$	$\kappa_\mathrm{s}\frac{\partial\vartheta_\mathrm{s}}{\partial y_\mathrm{s}}=k(\vartheta_\mathrm{b}-\vartheta_\mathrm{s})$	$\vartheta_\mathrm{s}=\vartheta_0$

ISBN: 978-0-9984188-3-4; Published online www.heatexchanger-fouling.com

Transport of hydroxide ions into the soil. Describing diffusion of water into the soil superimposed by diffusion of hydroxide ions is a multicomponent diffusion problem. Theoretically, it could be described using the Maxwell-Stefan-Diffusion equations [38, 39] or multicomponent Fickian diffusion equations [40]. These approaches are not of practical use since many parameters, like a diffusivity tensor, are required. In the context of foodstuff, diffusion of a cleaning fluid into a material has been described using only a single diffusion equation [27, 28, 41, 42]. This approach may be used for constant operating conditions. The present paper aims to provide a cleaning model that is able to capture multistep cleaning procedures, where, e.g., a soil is prewetted with cold water and subsequently cleaned with hot sodium hydroxide solution. For such cases, it is necessary to account for the transport of water and the transport of hydroxide ions separately. Both processes feature co-dependencies. If water containing hydroxide ions diffuses into the soil, the hydroxide ions are transported convectively with the water [43–45]. In case the soil is saturated with water, but hydroxide ions are present in the cleaning solution, no diffusion of water occurs. However, hydroxide ions can diffuse through the water within the soil, and the soil matrix itself acts as a hindrance. The latter scenario is well investigated in the context of ion diffusion within geological materials, where the apparent diffusion coefficient of hydroxide ions D_{OH^-} is modeled dependent on the water concentration [46]. As discussed in the introduction, there are also practical applications where a soil requires interaction with hydroxide ions before it becomes swellable [7, 9, 10, 20, 27, 28]. Such cases may also be captured using the present framework by setting the apparent diffusion coefficient of water D_{f} to zero as long as no hydroxide ions are present in the soil.

Based on the above considerations, the transport of hydroxide ions into the soil is now described using a convection diffusion equation

$$\frac{\mathrm{d}\Phi}{\mathrm{d}t} = -\int_{A_\mathrm{s}} \underline{J}_\mathrm{conv} \cdot \underline{n}\, \mathrm{d}A - \int_{A_\mathrm{s}} \underline{J}_\mathrm{diff} \cdot \underline{n}\, \mathrm{d}A. \quad (11)$$

Equation (11) is stated in terms of a conservative quantity Φ, since it will be reused later to describe the enthalpy conservation. The definitions of all quantities related to hydroxide ion transport are summarized in Tab. 1. Furthermore, the relationship between Φ and its density φ is given via

$$\Phi = \int_{V_\mathrm{s}} \varphi\, \mathrm{d}V. \quad (12)$$

The transport velocity $\underline{u}$ is determined using the diffusive flux of water into the soil by

$$\underline{u} = \frac{\underline{J}_\mathrm{f,diff}}{\rho_\mathrm{f}}. \quad (13)$$

Equation (11) is discretized in the same manner as Eq. (4). To obtain the interface values for discretizing the convection term, an upwind scheme is used. The apparent diffusion coefficient D_{OH^-} may be a function of $\beta_\mathrm{f}, \beta_{\mathrm{OH}^-}$ and ϑ_s. Equivalently to Eq. (8), the concentration of hydroxide ions β_{OH^-} can be determined from their mass and the cell height. The boundary conditions for the hydroxide ion concentration are similar to the boundary conditions for the water concentration. On the interface of soil and cleaning fluid, the hydroxide ion concentration of the bulk flow above the soil, $\beta_{\mathrm{b,OH}^-}$, is assumed. Note that the present framework is designed for small hydroxide ion concentrations so that the mass of hydroxide ions does not contribute significantly to the soil mass or volume, so that Eq. (2) and (3) are still valid.

Heat transfer into the soil. Heat transfer can be modelled according to Eq. (11) using the enthalpy stored in the soil H_s as conservative quantity Φ. All other terms of Eq. (11) are defined in Tab. 1. The enthalpy H_s is defined for the whole soil, assuming that the water and dry soil within a volume have the same temperature ϑ_s. Swelling only results from water moving between the cells so that the convective term only needs to account for the enthalpy transported by the water. The discretization is performed as shown in the previous section.

The boundary conditions for the soil temperature are more complex. On top, at $y_\mathrm{s} = h_\mathrm{s}$, convective heat transfer between the cleaning fluid and the soil is assumed, which is characterized by a heat transfer coefficient k and the bulk temperature of the main flow ϑ_b. At $y_\mathrm{s} = 0$, the soil is in contact with a substrate of the thickness δ_w, which typically has a high heat conductivity and absorbs heat from the soil. To account for this effect, a one-dimensional heat transfer equation

$$\frac{\partial \vartheta_\mathrm{w}}{\partial t} = a_\mathrm{w} \frac{\partial^2 \vartheta_\mathrm{w}}{\partial y_\mathrm{s}^2} \quad (14)$$

is solved in each segment for $y_\mathrm{s} \in [-\delta_\mathrm{w}, 0]$ to model the distribution of the wall temperature ϑ_w, with a_w the thermal diffusivity of the wall. For the present framework it is assumed that the wall is isolated at $y_\mathrm{s} = -\delta_\mathrm{w}$, yielding $\left.\frac{\partial \vartheta_\mathrm{w}}{\partial y}\right|_{y_\mathrm{s}=-\delta_\mathrm{w}} = 0$. The initial condition is given by $\vartheta_\mathrm{w}(y_\mathrm{s}, t=0) = \vartheta_0$. At the interface, the two problems are coupled: $\vartheta_\mathrm{s}(y_\mathrm{s}=0) = \vartheta_\mathrm{w}(y_\mathrm{s}=0)$ and $\kappa_\mathrm{s} \left.\frac{\partial \vartheta_\mathrm{s}}{\partial y_\mathrm{s}}\right|_{y_\mathrm{s}=0} = \kappa_\mathrm{w} \left.\frac{\partial \vartheta_\mathrm{w}}{\partial y_\mathrm{s}}\right|_{y_\mathrm{s}=0}$. Equation (14) is also solved numerically using a finite volume method with midpoint rule approximating the integrals, linear interpolation for the diffusive fluxes and the Euler-forward method for the temporal discretization.

ISBN: 978-0-9984188-3-4; Published online www.heatexchanger-fouling.com

Modeling of the cleaning mechanisms

Adhesive detachment. Adhesive detachment is modeled in accordance to previous model versions [11, 19]. Assuming the hydrodynamic load $\tau_{\mathrm{hyd},i}$ acting on a soil segment i is known, adhesive detachment takes place once the hydrodynamic load overcomes the adhesion between the soil and the substrate τ_{ad}. See Fig. 2 for the definition of those quantities. For the following equations, the index i is dropped, as in the previous section. It is assumed that the adhesion obeys the following dependencies

$$\tau_{\mathrm{ad}} = f(\beta_{\mathrm{f},1/2}, \beta_{\mathrm{OH^-},1/2}, \vartheta_{\mathrm{s},1/2}). \tag{15}$$

The index $1/2$ refers to the interface between soil and wall (Fig. 2). Soil removal by adhesive detachment is modeled by the removal criterion

$$N_y^{(n+1)} = \begin{cases} N_y^{(n)}, & C_{\mathrm{ad}}\tau_{\mathrm{hyd}} \leq \tau_{\mathrm{ad}} \\ 0, & C_{\mathrm{ad}}\tau_{\mathrm{hyd}} > \tau_{\mathrm{ad}}. \end{cases} \tag{16}$$

Criterion Eq. (16) removes all cells in case adhesive detachment takes place. If this happens, the soil height of a segment and its soil mass is set to zero. The critical stress τ_{ad} can, e.g., be measured in micromanipulation experiments [11, 13, 47, 48] or determined by fluid dynamic gauging [49]. In these experiments, the application of the load differs significantly from the load applied in the cleaning process. Therefore, the correction factor C_{ad} was introduced in previous publications [11, 13] to overcome these differences.

Cohesive separation. Cohesive separation is also modeled in accordance with the model presented in [13]. It occurs when the hydrodynamic load τ_{hyd} acting on a segment i (index i dropped) overcomes the cohesion between two different cells. Cohesion is assumed to have the same dependencies as adhesion, i.e.

$$\tau_{\mathrm{coh},j-1/2} = f(\beta_{\mathrm{f},j-1/2}, \beta_{\mathrm{OH^-},j-1/2}, \vartheta_{\mathrm{s},j-1/2}). \tag{17}$$

See Fig. 2 for definition of τ_{coh}. The removal criterion reads

$$N_y^{(n+1)} \begin{cases} N_y^{(n)}, \\ \text{if } C_{\mathrm{coh}}\tau_{\mathrm{hyd}} \leq \min_j(\tau_{\mathrm{coh},j-1/2}^{(n)}) \\ \min_j(\{j-1 |\, \tau_{\mathrm{coh},j-1/2}^{(n)} < C_{\mathrm{coh}}\tau_{\mathrm{hyd}}\}), \text{ else.} \end{cases} \tag{18}$$

The first condition in Eq. (18) is applied when the minimum of the cohesive stresses is still larger than the hydrodynamic load, and thus, no cells are removed. In case there is at least one cell interface, where the cohesion is overcome by the hydraulic load, the interface closest to the wall is chosen, and all cells above it are removed. If cells are removed from a segment by cohesive separation, they do not contribute to the soil mass or height of a segment anymore. The boundary conditions for the swelling and one-dimensional transport equations are passed down to the uppermost remaining cell.

Viscous shifting. In case of viscous shifting the soil flows and a linear velocity profile is assumed in each segment i reading

$$u_{\mathrm{s},i}(y_{\mathrm{s}}) = \dot{\gamma}_{\mathrm{s},i} y_{\mathrm{s}}. \tag{19}$$

Herein, $\dot{\gamma}_{\mathrm{s},i}$ is the shear rate and y_{s} the wall-normal coordinate. See Fig. 2 for definition of $u_{\mathrm{s},i}(y_{\mathrm{s}})$. The rheology of the soil is assumed to be of the form $\tau_{\mathrm{s}} = f(\dot{\gamma}_{\mathrm{s}}, \vartheta_{\mathrm{s}}, \beta_{\mathrm{f}}, \beta_{\mathrm{OH^-}})$. The shear rate within a segment $\dot{\gamma}_{\mathrm{s},i}$ is determined by solving

$$\tau_{\mathrm{hyd},i} = \tau_{\mathrm{s}} = f(\dot{\gamma}_{\mathrm{s},i}, \vartheta_{\mathrm{s},i}, \beta_{\mathrm{f},i}, \beta_{\mathrm{OH^-},i}), \tag{20}$$

where $\vartheta_{\mathrm{s},i}, \beta_{\mathrm{f},i}$ and $\beta_{\mathrm{OH^-},i}$ correspond to average values in segment i. The velocity profile determined in this way is then used to describe the transport of the conservative quantities listed in Tab. 1, i.e., the water mass m_{f}, the dry soil mass m_{d}, the mass of hydroxide ions $m_{\mathrm{OH^-}}$ and the enthalpy H_{s} between the segments. Since the existing formulation for viscous shifting from [14] was developed for a soil that is only discretized into segments, the formulation for the present work needs to be adjusted. The segments themselves are further partitioned into cells and conservative quantities must be evaluated cell-wise. The derivation is again presented for a conservative quantity Φ with a density φ. The steps described below are performed for all quantities listed in Tab. 1. Different from the swelling procedure, the soil mass is affected by viscous shifting since here the whole soil is flowable, not only the water within. When performing viscous shifting the change of Φ in cell i,j can be expressed as

$$\frac{\mathrm{d}\Phi_{i,j}}{\mathrm{d}t} = \dot{\Phi}_{i,j,\mathrm{in}} - \dot{\Phi}_{i,j,\mathrm{out}}. \tag{21}$$

Equation (21) can be discretized using the Euler-forward scheme reading

$$\Phi_{i,j}^{(n+1)} - \Phi_{i,j}^{(n)} = \Delta t(\dot{\Phi}_{i,j,\mathrm{in}}^{(n)} - \dot{\Phi}_{i,j,\mathrm{out}}^{(n)}). \tag{22}$$

The flux going out of a cell is, then, calculated from

$$\dot{\Phi}_{i,j,\mathrm{out}}^{(n)} = \int_{A_{i,j}} \varphi_{i,j}^{(n)} u_{\mathrm{s},i}^{(n)}(y_{\mathrm{s}}) \mathrm{d}A = W \int_{y_{\mathrm{s},i,j-1/2}^{(n)}}^{y_{\mathrm{s},i,j+1/2}^{(n)}} \varphi_{i,j}^{(n)} \dot{\gamma}_{\mathrm{s},i}^{(n)} y_{\mathrm{s}} \mathrm{d}y_{\mathrm{s}}. \tag{23}$$

Herein, $A_{i,j}$ is the surface area of the outlet of the cell i,j, shown in Fig. 4. The variables are illustrated in Fig. 4. For the second equality sign a two-dimensional problem of width W in cartesian coordinates is assumed. When using non-cartesian

ISBN: 978-0-9984188-3-4; Published online www.heatexchanger-fouling.com

coordinates, the surface integrals must be evaluated accordingly, as shown in [14].

In the next step the calculation of the flux into a cell, $\dot{\Phi}_{i,j,\mathrm{in}}^{(n)}$, is discussed. To ensure conservation, the amount flowing into segment i must be equivalent to the amount leaving segment $i-1$. The problem is, however, that the segments in general may have different heights and may also have different numbers of cells caused by cohesive separation. As a remedy, the inlet of cell in segment i is projected onto cell $i-1$. The projected y-positions can be obtained using $y_{\mathrm{s},i,j}^{(n),\mathrm{pr}} = (h_{\mathrm{s},i-1}^{(n)}/h_{\mathrm{s},i}^{(n)}) y_{\mathrm{s},i,j}^{(n)}$. The projection is sketched exemplarily depicted in Fig. 4. Using these relations, the flux into a cell is computed via

$$\dot{\Phi}_{i,j,\mathrm{in}}^{(n)} = \int_{A_{ij}^{\mathrm{pr}}} \varphi_{i-1}^{(n)}(y_\mathrm{s}) u_{\mathrm{s},i-1}^{(n)}(y_\mathrm{s}) \mathrm{d}A = W \int_{y_{\mathrm{s},i,j-1/2}^{(n),\mathrm{pr}}}^{y_{\mathrm{s},i,j+1/2}^{(n),\mathrm{pr}}} \varphi_{i-1}^{(n)}(y_\mathrm{s}) \dot{\gamma}_{\mathrm{s},i-1}^{(n)} y_\mathrm{s} \mathrm{d}y_\mathrm{s}. \quad (24)$$

The integration is usually performed across multiple cells of segment $i-1$. Hence, when evaluating the integral in Eq. (24) numerically, $\varphi_{i-1}(y_\mathrm{s})$ is replaced by the corresponding cell centered values.

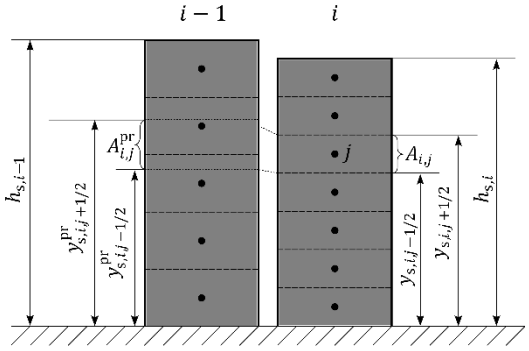

Fig. 4. Definition of quantities relevant for viscous shifting at cell i,j, projection of cell j from segment i on segment $i-1$. For better readability, the superscript (n) has been omitted for all quantities.

Computational algorithm

After initializing all quantities, the following operations are performed in each time step:

1. For each segment:
1.a) Calculate diffusion of water into the segment
1.b) Calculate hydroxide ion transport into the segment
1.c) Calculate heat transfer into the segment and the substrate
1.d) Update adhesion (Eq. (15)), cohesion (Eq. (17)) and soil rheology (Eq. (20))
1.e) Check for adhesive detachment using Eq. (16)
1.f) Check for cohesive separation using Eq. (18)
2. Perform viscous shifting by updating all conservative quantities listed in Tab. 1 using Eq. (22-24).

The model was implemented in Python (version 3.9.13). All computations were carried out on a laptop with 4 cores (Intel Core i5-6300, 2.4 GHz). Each calculation took less than 5 min.

VERIFICATION AND VALIDATION

Transport processes into the soil

Diffusion of water. To validate the diffusion of water into the soil, a reference case reported in [13] is investigated. Swelling of starch in water at 20 °C is studied for different initial soil mass coverages $m_{\mathrm{s},0}''$ and the evolution of soil height over time is monitored. In the reference, another diffusion model based on the water mass fraction $\omega_\mathrm{f} = m_\mathrm{f}/(m_\mathrm{f} + m_\mathrm{d})$ is proposed. For the water mass fraction, the initial value values $\omega_\mathrm{f}(y, t=0) = \omega_0 = 0.138$, the maximum water mass fraction $\omega_{\max} = 0.91$ and the dry density $\rho_\mathrm{d} = 1056.6\,\mathrm{kg/m^3}$ were determined experimentally [13]. Applying the definition of the water mass fraction, the necessary values for the present framework, $\beta_0 = 144.62\,\mathrm{kg/m^3}$ and $\beta_{\max} = 917.94\,\mathrm{kg/m^3}$, are determined. The swelling calculation was performed with a single segment and an initial resolution of $h_{\mathrm{s},i,j}^{(0)} = 5\,\mu\mathrm{m}$ was used. The diffusion coefficient was determined using a grid search [11, 13] to fit the experimental measurements. The best fit was achieved using an exponential ansatz for the diffusion coefficient $D_\mathrm{f} = D_{\mathrm{f},0}\exp(\alpha_\mathrm{f}\beta_\mathrm{f})$, where $D_{\mathrm{f},0} = 2.5 \cdot 10^{-11}\,\mathrm{m^2/s}$ and $\alpha_\mathrm{f} = 3.53 \cdot 10^{-3}\,\mathrm{m^3/kg}$. The results are displayed in Fig. 5. The model predicts almost the same heights as the previous one and results are within the error bars of the experiments. This validates the functionality of the newly formulated diffusion model.

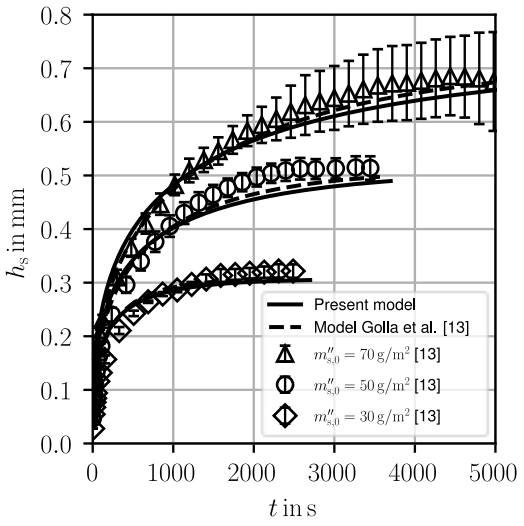

Fig. 5. Comparison of the evolution of soil height over time between the present diffusion model,

ISBN: 978-0-9984188-3-4; Published online www.heatexchanger-fouling.com

experimental data [13], and the diffusion model of [13].

Transport of hydroxide ions. To validate the diffusion model for the hydroxide ions a reference case by Wiese et al. [27] is investigated. In the reference, diffusion of hydroxide ions into a WPI gel was studied at different temperature levels. WPI is a proteinaceous soil, which requires reaction with hydroxide ions to become swellable. The penetration front of hydroxide, δ_{pen}, was made visible using the pH indicator molphthalein, triggered at $\mathrm{pH} \geq 9.3$. Apparent diffusion coefficients for the hydroxide ions of $D_{\mathrm{OH^-},20\,°\mathrm{C}} = 6.21 \cdot 10^{-11}\ \mathrm{m^2/s}$, $D_{\mathrm{OH^-},40\,°\mathrm{C}} = 7.89 \cdot 10^{-11}\ \mathrm{m^2/s}$ and $D_{\mathrm{OH^-},55\,°\mathrm{C}} = 11.4 \cdot 10^{-11}\ \mathrm{m^2/s}$ are reported and used for the present validation simulation. The hydroxide ion concentration in the cleaning fluid was $\beta_{\mathrm{b,OH^-}} = 0.01\ \mathrm{kg/m^3}$ [27]. Diffusion of water into the soil was not considered in the validation since the required quantities are not reported in the reference. The results are provided in Fig. 6. The results achieved with the present model are in agreement with the model used in the reference and the experimental data reported. The deviations for $\vartheta_{\mathrm{s}} = 55\,°\mathrm{C}$ are discussed in the reference. In the experiments, the penetration front is calculated with respect to the initial soil height and the change of soil height due to swelling or dissolving is neglected. These effects become more dominant with increasing fluid temperature. The results obtained validate the ability of the present model to compute the hydroxide ion distribution.

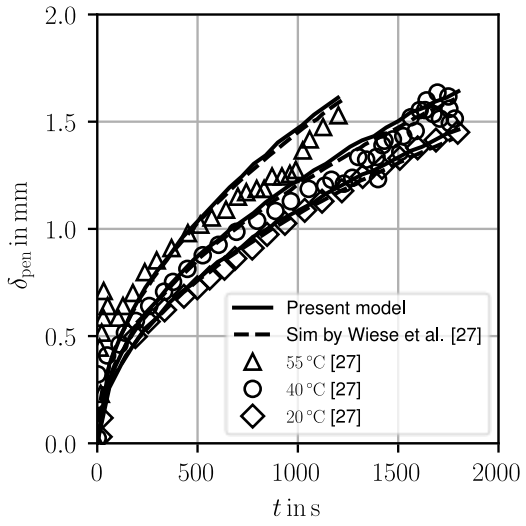

Fig. 6. Comparison of the evolution of hydroxide ion penetration front over time between the present diffusion model, experimental data [27], and the diffusion model presented in [27] there.

Thermal model. To validate the thermal model, a reference simulation was performed using the chtMultiRegionFoam solver of the OpenFOAM v7 library. Positioning of the soil and coordinate system are according to Fig. 2. The physical parameters used are inspired by the test rig described in [11], since it is used for cleaning experiments by the present authors. In the present validation simulation, the soil is immobile and has a length of $L_{\mathrm{s}} = 0.100\ \mathrm{m}$ with a height of $h_{\mathrm{s}} = 0.5\ \mathrm{mm}$. The wall has a thickness of $\delta_{\mathrm{w}} = 15\ \mathrm{mm}$ and is made of steel ($\kappa_{\mathrm{w}} = 15\ \mathrm{W/(m\,K)}$, $c_{p,\mathrm{w}} = 500\ \mathrm{J/(kg\,K)}$, $\rho_{\mathrm{w}} = 7900\ \mathrm{kg/m^3}$). The thermal properties of the soil employed here are inspired by Mahdi et al. [50]: $\kappa_{\mathrm{s}} = 0.5\ \mathrm{W/(m\,K)}$, $c_{p,s} = 2000\ \mathrm{J/(kg\,K)}$, $\rho_{\mathrm{s}} = 1030\ \mathrm{kg/m^3}$. The initial temperature was $\vartheta_0 = 20\,°\mathrm{C}$ and the bulk flow temperature was $\vartheta_{\mathrm{b}} = 60\,°\mathrm{C}$. A bulk flow velocity of $u_{\mathrm{b}} = 1\ \mathrm{m/s}$ was considered, resulting in a heat transfer coefficient of $k \approx 15000\ \mathrm{W/(m^2\,K)}$ [51]. In the present simulation a spatial resolution of $N_y = 20$ and $N_{y,\mathrm{w}} = 20$ was used for each soil segment ~~the soil~~ and wall, respectively. The simulation was conducted until $t_{\mathrm{end}} = 200\ \mathrm{s}$.

Results are now compared in terms of the dimensionless temperature $\Theta = [\vartheta(y_{\mathrm{s}} = 0) - \vartheta_{\mathrm{b}}]/[\vartheta_0 - \vartheta_{\mathrm{b}}]$ at the soil-substrate interface. The maximum deviation of Θ between the reference simulation and the present model is termed $\Delta\Theta$ and shown in Fig. 7 along the x-axis. Only half of the domain in x is shown due to symmetry. Since the present model uses a one-dimensional transport equation, the generated results are independent of x. In the reference simulation, however, two-dimensional effects and heating of the soil through the side are considered as well. The maximum deviation is, therefore, smaller than 0.1 for regions that are in the middle of the soil ($0.1 < \frac{x}{L_{\mathrm{s}}} < 0.9$). At $x = 0$ and $x = L_{\mathrm{s}}$ the simulations deviate the most, with $\Delta\Theta_{\mathrm{max}} \approx 0.42$. In a cleaning simulation, the soil would be discretized into segments and an average temperature within the segments would be considered. Therefore, the deviations obtained for an exemplary discretization with $N_{\mathrm{seg}} = 5$ is shown in Fig. 7 as well. It is seen that the worst deviations in segments 1 and 5 are $\Delta\Theta_{\mathrm{max}} = 0.12$, in this case. Considering the reduced computational effort when only accounting for one-dimensional transport in wall-normal direction, this is an acceptable error.

Cleaning mechanisms

Adhesive detachment. In the next step the combined model is validated by testing its ability to predict single cleaning mechanisms correctly, which is required, as these should all be covered adequately when combining them. For adhesive detachment, the experiments of Köhler et al. [11]

ISBN: 978-0-9984188-3-4; Published online www.heatexchanger-fouling.com

are used as a reference. Here, cleaning of a ketchup layer was investigated using water at 20 °C. Experiments were performed in a rectangular duct with a cross-section of 78 × 5 mm². One of the large walls was soiled with a thin layer of dried ketchup. Since only regions far away from the smaller side walls are considered, the flow in the region of interest corresponds to a plane channel flow. The diffusion parameter D_f, the function for adhesion (Eq. (15)), and the correction factor C_ad were parameterized for the present model using the experiments and procedure described in [11]. This results in $D_\mathrm{f} = D_{\mathrm{f},0}\beta_\mathrm{f}^{\alpha_\mathrm{f}}$, with $D_{\mathrm{f},0} = 2.2 \cdot 10^{-13}\ \mathrm{m}^{2+3\alpha_\mathrm{f}}/(\mathrm{s\ kg}^{\alpha_\mathrm{f}})$ and $\alpha_\mathrm{f} = 1.36$, $\tau_\mathrm{ad} = a\exp(b\beta_\mathrm{f})$, with $a = 811$ kPa and $b = -0.016\ \mathrm{m}^3/\mathrm{kg}$, and $C_\mathrm{ad} = 14.2$.

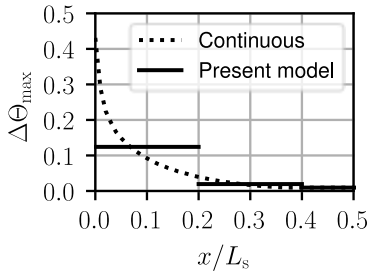

Fig. 7. Maximum deviation $\Delta\Theta_\mathrm{max}$ between the simulation performed with the present model and a reference simulation performed in OpenFOAM. The dotted line represents the error along the x-axis while the solid lines show the segment-wise deviation of the average temperature when discretizing the soil with $N_\mathrm{seg} = 5$ segments. Only half of the domain in x is shown due to symmetry.

In the cases shown, the initial soil mass coverage was kept at $m''_{\mathrm{s},0} = 278\ \mathrm{g/m^2}$ and the flow velocity was varied between $u_\mathrm{b} = 0.5\ \mathrm{m/s}$ and $u_\mathrm{b} = 2.0\ \mathrm{m/s}$. Simulations were carried out with one segment and the segment was discretized with $N_y = 25$ cells. The results are shown in Fig. 8 in terms of the cleaning time t_c. The present model reproduces the results of the reference model and experiments accurately.

Cohesive separation. The sub-model for cohesive separation is validated with data presented by Golla et al. [13]. Cleaning experiments and corresponding simulations were carried out for a starch layer in the same duct as considered in the previous section. The parameters of the diffusion model were already stated in the corresponding validation. The remaining parameters required to describe cohesive separation were determined as in [11, 13]: $\tau_\mathrm{coh} = a\exp(b\beta_\mathrm{f})$, with $a = 500$ MPa and $b = -0.021\ \mathrm{m}^3/\mathrm{kg}$ and $C_\mathrm{coh} = 0.67$.

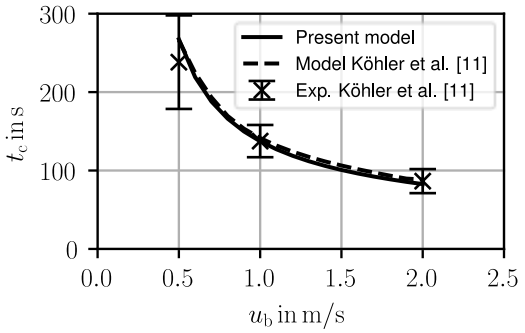

Fig. 8. Cleaning times for varying bulk velocities and comparison with reference data [11].

In the case presented in Fig. 9, an initial soil mass coverage of $m''_{\mathrm{s},0} \approx 50\ \mathrm{g/m^3}$ and a bulk velocity of $u_\mathrm{b} = 1\ \mathrm{m/s}$ were employed. To account for locally varying soil distribution, the method discussed in [13] with a standard deviation of the initial soil mass of $\sigma_{m''_{\mathrm{s},0}} = 5\ \mathrm{g/m^3}$ was used. The results are compared with respect to the total dry soil mass coverage over time. The present model performs slightly better than the previous one but both models tend to overestimate the time when cleaning starts. The linear decrease of soil mass and the decay at the end are well represented by both models. However, the slope of the decrease is slightly overestimated. Compared to the validation case for adhesive detachment, the present model does not exactly match the previous model. This is because in the case of cohesive separation, the whole distribution of water within the soil has an influence on the result, while in the case of adhesive detachment only, the boundary value plays a role. Since the swelling model was updated, it is likely that the distribution water within the soil is not the same in both cases.

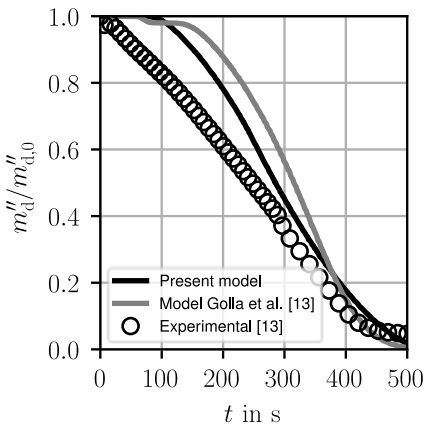

Fig. 9. Evolution of soil mass coverage over time for $u_\mathrm{b} = 1\ \mathrm{m/s}$ and $m''_{\mathrm{s},0} \approx (50 \pm 5)\ \mathrm{g/m^3}$.

Viscous shifting. To validate the new formulation of viscous shifting, the layer removal of chocolate by another chocolate in a straight pipe, radius $R =$

ISBN: 978-0-9984188-3-4; Published online www.heatexchanger-fouling.com

13 mm, length $L = 1$ m, under isothermal conditions at $\vartheta = 40$ °C was investigated. The setup was taken from Liebmann et al. [52], who performed numerical simulations of the flushing process using OpenFOAM. The case was already employed for the validation of the original model [14]. During the flushing process white chocolate is pushed out by the dark chocolate, hence white chocolate acts as cleaning fluid ($\rho_\mathrm{f} = 1260\ \mathrm{kg/m^3}$) and dark chocolate as soil ($\rho_\mathrm{d} = 1200\ \mathrm{kg/m^3}$). The rheology of the chocolates is described using the Windhab model [53], as described in [52, 54]. In the OpenFOAM simulation, the whole flushing procedure was simulated. A typical flushing process consists of a core removal and a layer removal phase [52]. The present framework can only be applied to the layer removal phase, when the height of the soil layer is sufficiently small. Hence, suitable initial conditions for the present modeling approach must be synthesized from the OpenFOAM simulation in terms of the initial soil heights. The procedure to do so is described in [14]. It was found that at $t_\mathrm{st} = 16.2$ s the soil layer was $h_\mathrm{s} < 0.1R$ and, hence, small enough to be simulated with the BCCM framework. At time t_st the initial values $h_{\mathrm{s},i}^0$ were taken. The hydrodynamic load for the present case was obtained from the analytical solution of single-phase flow in a pipe for a Windhab fluid [55, 56]. The bulk flow velocity of the main fluid was $u_\mathrm{b} = 0.1$ m/s. The present simulation was performed using $N_\mathrm{seg} = 5$ segments and $\Delta t = 0.1$ s, and the segments were initially discretized using $h_{\mathrm{s},i,j}^{(0)} = 0.02$ mm. The results obtained are shown in Fig. 10. As discussed in [14], the OpenFOAM simulations cannot be used for comparison if the soil height is below $h_{\mathrm{s},i}/R = 0.01$. Hence, these values are not shown in the diagram. The present model is able to reproduce the results obtained with the former model and matches the OpenFOAM reference.

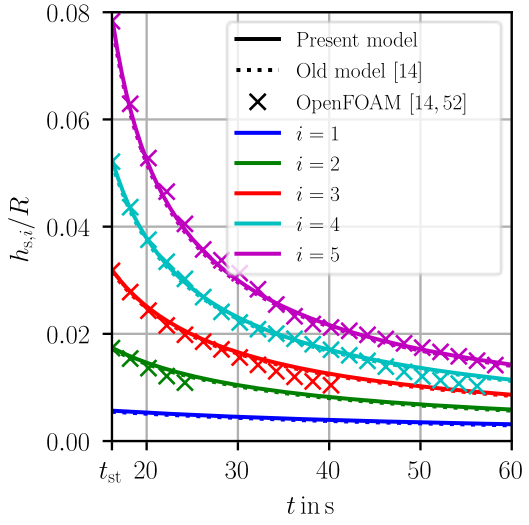

Fig. 10. Comparison of present results to former model results and resolved OpenFOAM simulations presented in [14, 52] in terms of evolution of soil height $h_{\mathrm{s},i}$ over time. The starting time is $t_\mathrm{st} = 16.2$ s. OpenFOAM results are only shown where $h_{\mathrm{s},i,\mathrm{OF}}/R > 0.01$.

Combined cleaning mechanisms. Finally, a verification is presented that the model is able to capture the simultaneous occurrence of cohesive separation, adhesive detachment and viscous shifting. To this end, a cleaning process at constant temperature using water as cleaning fluid was considered. The model parameters are fictional but inspired by the validation cases shown in the previous sections. The swelling parameters ($D_\mathrm{f}, \rho_\mathrm{f}, \rho_\mathrm{d}, \beta_0, \beta_\mathrm{max}$) and cohesive strength τ_coh are those of starch. For the adhesive strength, $\tau_\mathrm{ad} = a\exp(b\beta_\mathrm{f})$ with $a = 62.7$ kPa and $b = -0.009$ was used. The correction factors were set to $C_\mathrm{ad} = C_\mathrm{coh} = 1$. The soil rheology was described using a Newtonian fluid, i.e. $\tau_\mathrm{s} = \eta_\mathrm{s}\dot{\gamma}_\mathrm{s}$, with $\eta_\mathrm{s} = 1$ Pa s. The soil was discretized using $N_\mathrm{seg} = 5$ segments. Since focus of the present validation is the cleaning simulation, the hydrodynamic load of $\tau_{\mathrm{hyd},i} = 140$ Pa was imposed directly and identical for each segment. The initial soil heights were $h_{\mathrm{s},i}^{(0)} = ih_{\mathrm{s},1}^{(0)}$ with $h_{\mathrm{s},1}^{(0)} = 20$ µm and the segments were discretized with $h_{\mathrm{s},i,j}^{(0)} = 5$ µm, performing the simulation until $t_\mathrm{end} = 15$ s.

The results obtained are shown in Fig. 11 in terms of the evolution of segment heights over time. All cleaning mechanisms can be identified in the diagram: The steps correspond to cell removal due to cohesive separation, the continuous decrease of the soil height between steps is due to viscous shifting and the last cell is removed by adhesive detachment. Hence, the model is stable when all cleaning mechanisms occur simultaneously.

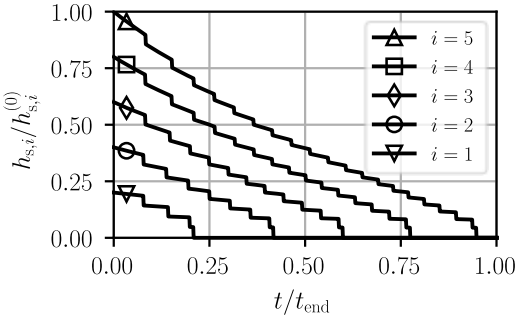

Fig. 11. Evolution of soil height over time for simultaneous occurrence of cohesive separation, adhesive detachment, and viscous shifting.

ISBN: 978-0-9984188-3-4; Published online www.heatexchanger-fouling.com

CASE STUDY: COMPLEX SOIL IN HEAT EXCHANGER

Setup

To demonstrate the capabilities of the proposed model, a fictional cleaning optimization study was performed, inspired by the cleaning of a soil in a HEX for dairy processing. Note, that the present study makes gross simplifications about the soil behavior. Detailed information about soils forming in HEX can be found, e.g., in [8, 57–59]. The soil is inspired by a so-called type A deposit [8, 9, 58, 59], which forms in a HEX at temperatures of $75-110$ °C and mostly consists of protein $(50-70\%)$ and minerals. Hence, interaction with hydroxide ions is required to make the soil swellable.

Typically, a CIP procedure consists of the following steps [1]: i) Prerinse, to remove loosely bound soil, ii) Detergent phase (alkali or acid), to remove soil layers, iii) Intermediate rinse to remove chemical, iv) Sanitization or disinfection, v) final water rinse. In some cases, steps ii) and iii) are performed twice: The first time with an alkaline solution to remove proteinaceous soils and the second time with an acidic solution to remove minerals. The present modeling for film-like soils addresses mainly parts ii) and iii) performed with an alkaline solution. Extending the present approach towards an acidic cleaning step would require solving another transport equation for hydronium ions and describing the material properties dependent on the hydronium ion concentration. For the present study, a simplified two-stage cleaning procedure was used, shown in Fig. 12. In the first stage, the soil is prewetted using sodium hydroxide solution as cleaning fluid to reduce the strength of the soil. In this stage, the cleaning fluid stands still, and no hydrodynamic load is applied. In the second stage, rinsing with clear water at constant bulk velocity is performed so that a constant hydrodynamic load τ_{hyd} acts on the soil. The suggested procedure bears the advantage that no water is wasted in the first stage, and the binding forces in the soil are still reduced. The time of the switch between the two stages is denoted with t_{sw}. As a surrogate for a possible real-life application the effect of varying t_{sw} on the cleaning time t_{c} and the required amount of water is studied. To this end, two different, constant bulk flow temperatures $\vartheta_{\mathrm{b},1}$ and $\vartheta_{\mathrm{b},2}$ are considered.

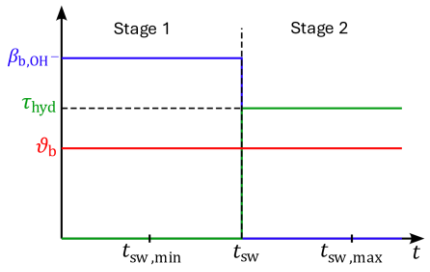

Fig. 12. Operating conditions of the simulated two-stage cleaning procedure, with the respective values provided in the text.

The temperature dependent diffusion coefficient for hydroxide ions was taken from [27] giving $D_{\mathrm{OH^-}}/(\mathrm{m^2/s}) = 3.6\cdot 10^{-14}(\vartheta/°\mathrm{C})^2 - 1.3\cdot 10^{-13}(\vartheta/°\mathrm{C}) + 7.2\cdot 10^{-12}$. To model the dependence of the diffusion coefficient of the water on the hydroxide ion concentration

$$D_{\mathrm{f}} = \begin{cases} 0, & \beta_{\mathrm{OH^-}} < \beta_{\mathrm{OH^-,crit}} \\ \frac{(\beta_{\mathrm{OH^-}}-\beta_{\mathrm{OH^-,crit}})}{(\beta_{\mathrm{b,OH^-}}-\beta_{\mathrm{OH^-,crit}})} D_{\mathrm{OH^-}}, & \beta_{\mathrm{OH^-}} \geq \beta_{\mathrm{OH^-,crit}} \end{cases} \quad (24)$$

was used. When the hydroxide ion concentration is smaller than the critical concentration $\beta_{\mathrm{OH^-,crit}}$, the diffusion coefficient remains zero. Once the critical concentration is surpassed, the diffusion coefficient increases linearly towards the value of the hydroxide ion diffusion coefficient. The critical concentration is assumed to be $\beta_{\mathrm{OH^-,crit}} = 0.5\beta_{\mathrm{b,OH^-}}$, where the bulk hydroxide ion concentration is $\beta_{\mathrm{b,OH^-}} = 0.01\ \mathrm{kg/m^3}$. The initial soil height was $h_{\mathrm{s}}^{(0)} = 1$ mm, and it was assumed that the soil has the same density as water, i.e, $\rho_{\mathrm{f}} = \rho_{\mathrm{d}} = 1000\ \mathrm{kg/m^3}$. The initial and maximum water concentration were $\beta_0 = 200\ \mathrm{kg/m^3}$ and $\beta_{\max} = 800\ \mathrm{kg/m^3}$, respectively. The thermal properties of the soil and wall were the same as in the validation case for the thermal model. The wall thickness was $\delta_{\mathrm{w}} = 3$ mm. The common initial temperature of soil and wall was $\vartheta_0 = 20$ °C, and the bulk flow temperatures $(\vartheta_{\mathrm{b},1}, \vartheta_{\mathrm{b},2}) = (60, 70)$ °C.

To model the cohesive strength, an ansatz $\tau_{\mathrm{coh}}(\vartheta_{\mathrm{s}}, \beta_{\mathrm{OH^-}}, \beta_{\mathrm{f}}) = a(\vartheta_{\mathrm{s}})\exp(b(\beta_{\mathrm{OH^-}})\beta_{\mathrm{f}})$ is used. The coefficients depend on temperature and hydroxide ion concentration, respectively. The temperature dependent coefficient a was modelled using another exponential ansatz, $a(\vartheta_{\mathrm{s}}) = a_1\exp(-a_2\vartheta_{\mathrm{s}})$, motivated by the well-known Arrhenius dependency. The two constants were calculated as follows. First the special case of $\beta_{\mathrm{OH^-}} = \beta_{\mathrm{OH^-,crit}}$ was considered, where the soil just becomes swellable. In this case, the soil should just be able to be removed, hence $\tau_{\mathrm{coh}}(\vartheta_{\mathrm{s}} = \vartheta_1, \beta_{\mathrm{OH^-}} = \beta_{\mathrm{OH^-,crit}}, \beta_{\mathrm{f}} = \beta_{\max}) = \tau_{\mathrm{hyd}}$. Furthermore, the effect of increasing the temperature was directly modelled using $\tau_{\mathrm{coh}}(\vartheta_{\mathrm{s}} = \vartheta_0, \beta_{\mathrm{OH^-}}, \beta_{\mathrm{f}}) = C_\vartheta\tau_{\mathrm{coh}}(\vartheta_{\mathrm{s}} = \vartheta_1, \beta_{\mathrm{OH^-}}, \beta_{\mathrm{f}})$. The coefficient b was modelled using a linear relationship $b(\beta_{\mathrm{OH^-}}) = -b_1\beta_{\mathrm{OH^-}}$, where b_1 was determined from $\tau_{\mathrm{coh}}(\vartheta_{\mathrm{s}}, \beta_{\mathrm{OH^-}} = \beta_{\mathrm{OH^-,crit}}, \beta_{\mathrm{f}}) = C_{\mathrm{OH^-}}\tau_{\mathrm{coh}}(\vartheta_{\mathrm{s}}, \beta_{\mathrm{OH^-}} = \beta_{\mathrm{b,OH^-}}, \beta_{\mathrm{f}})$. The way the cohesive strength is modelled introduces two parameters, C_ϑ and $C_{\mathrm{OH^-}}$, which directly regulate the sensitivity of the cohesive strength to a change of temperature or hydroxide ion concentration, respectively. To keep the number of parameters

ISBN: 978-0-9984188-3-4; Published online www.heatexchanger-fouling.com

manageable, $\tau_{\mathrm{ad}} = \tau_{\mathrm{coh}}$ was assumed. The soil rheology was characterized using

$$\dot{\gamma} = \begin{cases} 0, & \beta_{\mathrm{OH^-}} < \beta_{\mathrm{OH^-,crit}} \\ \tau_{\mathrm{hyd}}/\eta_{\mathrm{s}}(\vartheta_{\mathrm{s}}) & \beta_{\mathrm{OH^-}} \geq \beta_{\mathrm{OH^-,crit}}. \end{cases} \quad (25)$$

Below the critical hydroxide ion concentration $\beta_{\mathrm{OH^-,crit}}$ it was assumed that the soil is not able to flow. Above the critical concentration the dynamic viscosity decreases exponentially with the temperature, described by $\eta_{\mathrm{s}}(\vartheta_{\mathrm{s}}) = \eta_0 \exp(-c\,\vartheta_{\mathrm{s}})$, where $\eta_0 = 1$ Pa, and the parameter c is, again, determined by $\eta_{\mathrm{s}}(\vartheta_0) = C_\eta \eta_{\mathrm{s}}(\vartheta_1)$. The present study was performed using $\tau_{\mathrm{hyd}} = 10$ Pa, $C_\vartheta = 1.44$, $C_{\mathrm{OH^-}} = 1.5$, and $C_\eta = 2.0$. The soil was discretized using $N_{\mathrm{seg}} = 5$ segments and $N_{y,i} = 10$ cells per segment.

Results

By analyzing the suggested cleaning procedure, a minimum and a maximum switch time can be found. The time necessary for the soil-substrate interface to barely reach the critical hydroxide ion concentration $\beta_{\mathrm{OH^-,crit}}$ is the minimum switch time $t_{\mathrm{sw,min}}$ necessary so that complete cleaning can occur. On the other hand, the maximum reasonable switch time $t_{\mathrm{sw,max}}$ corresponds to the time the soil layer needs to be entirely swollen and heated up during stage 1. In that case the soil-substrate interface reaches the maximum water concentration β_{max} and the bulk fluid temperature ϑ_{b}, respectively. Remaining longer than $t_{\mathrm{sw,max}}$ in stage 1 would not change the outcome of the simulation. In case of $\vartheta_{\mathrm{b}} = 60$ °C and 70 °C, the minimum necessary switch times were found to be 6150 s and 2250 s, respectively, and the maximum reasonable switch times 7200 s and 3500 s, respectively, varying the switch time in steps of 50 s. For $\vartheta_{\mathrm{b,1}} = 60$ °C, the optimal switch time to minimize the cleaning time was found to be 7100 s, resulting in $t_{\mathrm{c,min}} = 7112$ s. For $\vartheta_{\mathrm{b,2}} = 70$ °C, on the other hand, the minimal cleaning time of $t_{\mathrm{c,min}} = 3155$ s was found with $t_{\mathrm{sw}} = 2600$ s. In all simulations, cohesive separation was the dominant cleaning mechanism. To compare both temperature levels, the switch time is non-dimensionalized using $t^*_{\mathrm{sw}} = (t_{\mathrm{sw}} - t_{\mathrm{sw,min}})/(t_{\mathrm{sw,max}} - t_{\mathrm{sw,min}})$. The results are shown in Fig. 13. For both temperature levels, the ratio $t_{\mathrm{c}}/t_{\mathrm{c,min}}$ rapidly decreases for $0 \leq t^*_{\mathrm{sw}} \leq 0.25$. After reaching the individual minima, the cleaning time increases again with increasing switch time. For cases where the soil is entirely swollen, the hydrodynamic load removes the soil as soon as it is applied. In these cases, the least amount of water is used, so the optimum in terms of water consumption can be found at $t^*_{\mathrm{sw}} \geq 1$. For $\vartheta_{\mathrm{b,2}} = 70$ °C , in contrast, the optimum in terms of cleaning time lies at $t^*_{\mathrm{sw}} = 0.28$ which demonstrates that even in this very small fictitious study, the optima for different questions can diverge.

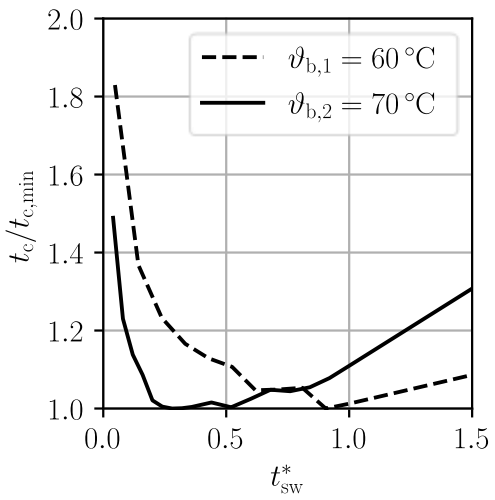

Fig. 13. Result of the cleaning optimization study in terms of cleaning time over dimensionless switch time, defined as $t^*_{\mathrm{sw}} = (t_{\mathrm{sw}} - t_{\mathrm{sw,min}})/(t_{\mathrm{sw,max}} - t_{\mathrm{sw,min}})$.

CONCLUSIONS

In the present paper, a combined cleaning model was proposed accounting for three different cleaning mechanisms at once: cohesive separation, adhesive detachment, and viscous shifting. The model contains sub-models for the transport of heat and hydroxide ions into the soil layer and its interaction with the binding forces of the soil. The transition between the cleaning mechanisms is not modeled directly. In fact, the apparent cleaning mechanism is a result of the simulation. Thorough validation of the new model with reference data was performed for all cleaning mechanisms covered. Furthermore, it was demonstrated that the new model is able to represent the three cleaning mechanisms covered simultaneously. Finally, a fictional case study of cleaning a typical soil forming in a HEX was devised, in which several cleaning mechanisms are involved. A simplified CIP procedure consisting of a prewetting stage, and a rinsing stage was simulated using the present model. Although soil parameters were fictional, the study indicates resource-saving potential by using prewetting and demonstrates the potential of the present model to perform realistic optimization studies.

At this point, the model does not include the cleaning mechanism characterized by diffusive dissolution, so that the removal of such soils cannot be described, which mainly applies to mineral soils. However, a reasonable estimate can be made by applying the sub-model for cohesive separation with very small particles.

ISBN: 978-0-9984188-3-4; Published online www.heatexchanger-fouling.com

While the model was formulated here using a transport equation for hydroxide ions, this could also be done for hydronium ions to account for acidic cleaning, which is required to remove mineral soils. Hence, a reasonable next step would be to extend the model to also involve transport equations for other chemicals. However, this also requires to describe the soil properties as a function of the concentration of these chemicals.

In the present study, a combined cleaning model was developed and implemented. A validation with real experimental data of a complex case could not be presented. This is very difficult because such a validation requires a comprehensive characterization of the soil, i.e., describing the cohesion, the adhesion, and the soil rheology depending on the water and hydroxide ion concentration as well as the temperature. Such a characterization is cumbersome and left for future work.

Currently very few methods are available that can be used to determine the parameters required by the model for realistic soils, such as soils forming in heat exchangers. A promising approach would be to apply iterative reverse engineering to estimate model parameters. Due to the very short calculation times, a larger number of parameter combinations can be tested in reasonable time.

This would also pave the way towards even more realistic and more complex cleaning optimization studies.

ACKNOWLEDGEMENTS

This research project is supported by the Industrievereinigung für Lebensmitteltechnologie und Verpackung e.V. (IVLV), the Arbeitsgemeinschaft industrieller Forschungs-vereinigungen „Otto von Guericke“ e.V. (AiF) and the Federal Ministry of Economic Affairs and Climate Action (IGF 21334 BR). The authors are grateful to the Center for Information Services and High Performance Computing [Zentrum für Informationsdienste und Hochleistungsrechnen (ZIH)] at TU Dresden for providing its facilities for high throughput calculations. CG thanks Ricardo Rebel for helping to run the simulations on HPC.

NOMENCLATURE

Latin symbols

A	Area, m^2
a	Constant, $-$
b	Constant, $-$
C	Constant, $-$
c	Constant, $-$
c_p	Heat capacity, $\mathrm{J/(kg\ K)}$
D	Diffusivity, m^2/s
D_0	Diffusion model parameter, $-$
H	Enthalpy, J
h	Height, m
J	Flux, $-$
$\underline{J}$	Flux vector, $-$
k	Heat convection coefficient, $\mathrm{W/(m^2\ K)}$
L	Length, m
m	Mass, kg
m''	Mass coverage, $\mathrm{kg/m^2}$
$\dot{m}$	Mass flow, $\mathrm{kg/s}$
N	Number of, $-$
$\underline{n}$	Normal vector, $-$
R	Radius, m
t	Time, s
u	Flow velocity, $\mathrm{m/s}$
$\underline{u}$	Velocity vector, $\mathrm{m/s}$
V	Volume, m^3
W	Width, m
x	Spatial coordinate, m
y	Wall normal coordinate, m

Greek symbols

α	Diffusion model parameter, $-$
β	Mass concentration, $\mathrm{kg/m^3}$
$\dot{\gamma}$	Shear rate, $1/\mathrm{s}$
Δt	Time step, s
δ	Depth, m
η	Dynamic viscosity, Pa s
Φ	Conservative quantity, $-$
φ	Density of Φ, $-$
κ	Heat conduction coefficient, $\mathrm{W/(m\ K)}$
ρ	Density, $\mathrm{kg/m^3}$
σ	Standard deviation, $-$
Θ	Dimensionless temperature, $-$
ϑ	Temperature, ℃
τ	Shear stress, Pa
τ_{ad}	Adhesive strength, Pa
τ_{coh}	Cohesive strength, Pa
τ_{hyd}	Hydraulic load, Pa
$\underline{\underline{\tau}}$	Shear stress tensor, Pa
ω	Mass fraction, kg/kg

Sub- and superscripts

ad	Adhesion
b	Bulk
chr	Characteristic
coh	Cohesion
conv	Convective
d	Dry
diff	Diffusive
end	End
f	Fluid, water
i	Index for spatial discretization
in	In
int	Interface
j	Index for spatial discretization
max	Maximum
min	Minimum
n	Index for temporal discretization
$\mathrm{OH^-}$	Hydroxide

ISBN: 978-0-9984188-3-4; Published online www.heatexchanger-fouling.com

out	Out
pen	Penetration
s	Soil
seg	Segments
st	Start
sw	Switch
w	Wall
0	Initial value
∗	Dimensionless

Abbreviations

BCCM	Boundary condition cleaning model
CFD	Computational fluid dynamics
CIP	Cleaning-in-place
HEX	Heat exchanger
pH	Potential of hydrogen
WPC	Whey protein concentrate
WPI	Whey protein isolate

REFERENCES

[1] Goode, K. R., Asteriadou, K., Robbins, P. T., and Fryer, P. J., Fouling and Cleaning Studies in the Food and Beverage Industry Classified by Cleaning Type, *Comprehensive Reviews in Food Science and Food Safety*, vol. 12, pp. 121–143, 2013.

[2] Landel, J. R., and Wilson, D. I., The fluid mechanics of cleaning and decontamination of surfaces, *Annual Review of Fluid Mechanics*, vol. 53, pp. 147–171, 2021.

[3] Pettigrew, L., Blomenhofer, V., Hubert, S., Groß, F., and Delgado, A., Optimisation of water usage in a brewery clean-in-place system using reference nets, *Journal of Cleaner Production*, vol. 87, pp. 583–593, 2015.

[4] Gésan-Guiziou, G., Sobańtka, A. P., Omont, S., Froelich, D., Rabiller-Baudry, M., Thueux, F., Beudon, D., Tregret, L., Buson, C., and Auffret, D., Life Cycle Assessment of a milk protein fractionation process: Contribution of the production and the cleaning stages at unit process level, *Separation and Purification Technology*, vol. 224, pp. 591–610, 2019.

[5] Wilson, D. I., Challenges in Cleaning: Recent Developments and Future Prospects, *Heat Transfer Engineering*, vol. 26, pp. 51–59, 2005.

[6] Tamime, A. Y., *Cleaning-in place: dairy, food and beverage operations*, 3rd ed., Blackwell Pub, Oxford, UK 2008.

[7] Xin, H., Chen, X. D., and ÖZkan, N., Whey Protein-Based Gel as a Model Material for Studying Initial Cleaning Mechanisms of Milk Fouling, *Journal of Food Science*, vol. 67, pp. 2702–2711, 2002.

[8] Fryer, P. J., Belmar-Beiny, M. T., and Schreier, P. J. R., Fouling and Cleaning: Mechanisms and Models, in: Yano, T., Matsuno, R., Nakamura, K. (Eds.), *Developments in Food Engineering*, Springer US, Boston, MA 1994, pp. 24–29.

[9] Fryer, P. J., Christian, G. K., and Liu, W., How hygiene happens: physics and chemistry of cleaning, *International Journal of Dairy Technology*, vol. 59, pp. 76–84, 2006.

[10] Gillham, C. R., Fryer, P. J., Hasting, A. P. M., and Wilson, D. I., Cleaning-in-Place of Whey Protein Fouling Deposits, *Food and Bioproducts Processing*, vol. 77, pp. 127–136, 1999.

[11] Köhler, H., Liebmann, V., Golla, C., Fröhlich, J., and Rüdiger, F., Modeling and CFD-simulation of cleaning process for adhesively detaching film-like soils with respect to industrial application, *Food and Bioproducts Processing*, vol. 129, pp. 157–167, 2021.

[12] Joppa, M., Köhler, H., Rüdiger, F., Majschak, J.-P., and Fröhlich, J., Experiments and simulations on the cleaning of a swellable soil in plane channel flow, *Heat Transfer Engineering*, vol. 38, pp. 786–795, 2017.

[13] Golla, C., Köhler, H., Fröhlich, J., and Rüdiger, F., Numerical modeling of a cohesively separating soil layer in consideration of locally varying soil distribution, *Heat and Mass Transfer*, 2023.

[14] Golla, C., Liebmann, V., Rebel, R., Köhler, H., Fröhlich, J., and Rüdiger, F., Numerical model for the cleaning of a film-like soil by viscous shifting under non-isothermal conditions, in: *Proceedings of 15th International Conference on Heat Exchanger Fouling and Cleaning 2024*, Lisbon, Portugal 2024.

[15] Golla, C., Boddin, L., Helbig, M., Köhler, H., Rudiger, F., and Fröhlich, J., Investigating the cleaning mechanism of film-like soils using fully convolutional networks, *Food and Bioproducts Processing*, 2024.

[16] Köhler, H., Liebmann, V., Joppa, M., and Fröhlich, J., On the concept of CFD-based prediction of cleaning for film-like soils, in: *Proceedings of 13th International Conference on Heat Exchanger Fouling and Cleaning 2019*, Warsaw, Poland 2019.

[17] Joppa, M., Köhler, H., Kricke, S., Majschak, J.-P., Fröhlich, J., and Rüdiger, F., Simulation of jet cleaning: diffusion model for swellable soils, *Food and Bioproducts Processing*, vol. 113, pp. 168–176, 2019.

[18] Joppa, M., Köhler, H., Rüdiger, F., Majschak, J.-P., and Fröhlich, J., Prediction of cleaning by means of computational fluid dynamics: implication of the pre-wetting of a swellable soil, *Heat Transfer Engineering*, vol. 41, pp. 178–188, 2020.

[19] Golla, C., Köhler, H., Liebmann, V., Fröhlich, J., and Rüdiger, F., CFD-based three-dimensional modeling of an adhesively detaching soil layer in a channel flow with sudden expansion, in: *Fouling and Cleaning in Food Processing 2022*, Lille, France 2022.

ISBN: 978-0-9984188-3-4; Published online www.heatexchanger-fouling.com

[20] Xin, H., Chen, X. D., and Özkan, N., Removal of a model protein foulant from metal surfaces, *AIChE Journal*, vol. 50, pp. 1961–1973, 2004.
[21] Fryer, P. J., and Asteriadou, K., A prototype cleaning map: A classification of industrial cleaning processes, *Trends in Food Science & Technology*, vol. 20, pp. 255–262, 2009.
[22] Christian, G. K., Cleaning of carbohydrate and dairy protein deposits, School of Chemical Engineering: University of Birmingham, United Kingdom, 2004.
[23] Cole, P. A., Asteriadou, K., Robbins, P. T., Owen, E. G., Montague, G. A., and Fryer, P. J., Comparison of cleaning of toothpaste from surfaces and pilot scale pipework, *Food and Bioproducts Processing*, vol. 88, pp. 392–400, 2010.
[24] Pereira, A., Mendes, J., and Melo, L. F., Monitoring cleaning-in-place of shampoo films using nanovibration technology, *Sensors and Actuators B: Chemical*, vol. 136, pp. 376–382, 2009.
[25] Goode, K. R., Asteriadou, K., Fryer, P. J., Picksley, M., and Robbins, P. T., Characterising the cleaning mechanisms of yeast and the implications for Cleaning In Place (CIP), *Food and Bioproducts Processing*, vol. 88, pp. 365–374, 2010.
[26] Le Gentil, C., Sylla, Y., and Faille, C., Bacterial re-contamination of surfaces of food processing lines during cleaning in place procedures, *Journal of Food Engineering*, vol. 96, pp. 37–42, 2010.
[27] Wiese, H., Geißler, H., Augustin, W., and Scholl, S., Diffusive mass transfer and protein removal in the alkaline cleaning of a jellylike whey protein fouling layer, *Heat and Mass Transfer*, 2023.
[28] Mercadé-Prieto, R., Paterson, W. R., Dong Chen, X., and Wilson, D. I., Diffusion of NaOH into a protein gel, *Chemical Engineering Science*, vol. 63, pp. 2763–2772, 2008.
[29] Jeurnink, T. J. M., and Brinkman, D. W., The cleaning of heat exchangers and evaporators after processing milk or whey, *International Dairy Journal*, vol. 4, pp. 347–368, 1994.
[30] Fan, L., Chen, X. D., and Mercadé-Prieto, R., On the nature of the optimum cleaning concentration for dairy fouling: High NaOH concentrations inhibit the cleavage of non-covalent interactions in whey protein aggregates, *LWT*, vol. 101, pp. 519–525, 2019.
[31] Peppas, N. A., Wu, J. C., and Von Meerwall, E. D., Mathematical Modeling and Experimental Characterization of Polymer Dissolution, *Macromolecules*, vol. 27, pp. 5626–5638, 1994.
[32] Aziz, N., Factors that affect cleaning process efficiency, School of Chemical Engineering: University of Birmingham, United Kingdom, 2008.
[33] Golla, C., Marschall, W. F., Kricke, S., Rüdiger, F., Köhler, H., and Fröhlich, J., Identification of cleaning mechanism by using neural networks, *Food and Bioproducts Processing*, vol. 138, pp. 86–102, 2023.
[34] Helbig, M., Föste, H., Augustin, W., and Scholl, S., Description of the cleaning mechanism of a model food soil using an optical detection method and the FDG technique, in: *Proceedings of 11th International Conference on Heat Exchanger Fouling and Cleaning 2015*, Dublin, Ireland 2015, pp. 256–263.
[35] Helbig, M., Zahn, S., Böttcher, K., Rohm, H., and Majschak, J.-P., Laboratory methods to predict the cleaning behaviour of egg yolk layers in a flow channel, *Food and Bioproducts Processing*, vol. 113, pp. 108–117, 2019.
[36] Kricke, S., Böttcher, K., Zahn, S., Majschak, J.-P., and Rohm, H., Effect of Physicochemical Properties of Native Starches on Cleaning in Falling Film and Plane Channel Flow Experiments, *Heat Transfer Engineering*, vol. 43, pp. 1416–1425, 2022.
[37] Crank, J., *The mathematics of diffusion*, 2d ed, Clarendon Press, Oxford 1975.
[38] Maxwell, J. C., On the Dynamical Theory of Gases, *Philosophical Transactions of the Royal Society of London*, vol. 15, pp. 49–88, 1867.
[39] Stefan, J., Über das Gleichgewicht und die Bewegung, insbesondere die Diffusion von Gasgemengen., n.d.
[40] Tyrrell, H. J. V., and Harris, K. R., The Phenomenology of diffusion, in: *Diffusion in Liquids*, Elsevier, 1984, pp. 56–76.
[41] Gekas, V., Öste, R., and Lamberg, I., Diffusion in Heated Potato Tissues, *Journal of Food Science*, vol. 58, pp. 827–831, 1993.
[42] Chavez, M. S., Luna, J. A., and Garrote, R. L., Apparent diffusion coefficient determination of sodium hydroxide through potato skin and flesh under different temperatures and concentration conditions, *Journal of Food Engineering*, vol. 30, pp. 377–388, 1996.
[43] Turhan, M., and Kaletunç, G., Modeling of Salt Diffusion in White Cheese during Long-Term Brining, *Journal of Food Science*, vol. 57, pp. 1082–1085, 1992.
[44] Papanu, J. S., Soane (Soong), D. S., Bell, A. T., and Hess, D. W., Transport models for swelling and dissolution of thin polymer films, *Journal of Applied Polymer Science*, vol. 38, pp. 859–885, 1989.
[45] Ranade, V. V., and Mashelkar, R. A., Convective diffusion from a dissolving polymeric particle, *AIChE Journal*, vol. 41, pp. 666–676, 1995.

ISBN: 978-0-9984188-3-4; Published online www.heatexchanger-fouling.com

[46] Tokunaga, T. K., Finsterle, S., Kim, Y., Wan, J., Lanzirotti, A., and Newville, M., Ion Diffusion Within Water Films in Unsaturated Porous Media, *Environmental Science & Technology*, vol. 51, pp. 4338–4346, 2017.
[47] Liu, W., Christian, G. K., Zhang, Z., and Fryer, P. J., Development and use of a micromanipulation technique for measuring the force required to disrupt and remove fouling deposits, *Food and Bioproducts Processing*, vol. 80, pp. 286–291, 2002.
[48] Zhang, Z., Ferenczi, M. A., Lush, A. C., and Thomas, C. R., A novel micromanipulation technique for measuring the bursting strength of single mammalian cells, *Applied Microbiology and Biotechnology*, vol. 36, pp. 208–210, 1991.
[49] Hooper, R. J., Liu, W., Fryer, P. J., Paterson, W. R., Wilson, D. I., and Zhang, Z., Comparative studies of fluid dynamic gauging and a micromanipulation probe for strength measurements, *Food and Bioproducts Processing*, vol. 84, pp. 353–358, 2006.
[50] Mahdi, Y., Mouheb, A., and Oufer, L., A dynamic model for milk fouling in a plate heat exchanger, *Applied Mathematical Modelling*, vol. 33, pp. 648–662, 2009.
[51] Baehr, H. D., and Stephan, K., *Heat and mass-transfer*, 2nd rev. ed, Springer, Berlin New York 2006.
[52] Liebmann, V., Heide, M., Köhler, H., Rüdiger, F., and Fröhlich, J., Improving flushing processes through targeted control of the temperature boundary conditions, *Proceedings in Applied Mathematics and Mechanics*, vol. 23, pp. e202300253, 2023.
[53] Eischen, J.-C., and Windhab, E. J., Viscosity of Cocoa and Chocolate Products, *Applied Rheology*, vol. 12, pp. 32–34, 2002.
[54] Liebmann, V., Heide, M., Köhler, H., Golla, C., Fröhlich, J., and Rüdiger, F., Reduced cleaning model for highly viscous non-Newtonian fluids in pipelines, *Computer Aided Chemical Engineering*, vol. 52, pp. 325–330, 2023.
[55] Petitjeans, P., and Maxworthy, T., Miscible displacements in capillary tubes. Part 1. Experiments, *Journal of Fluid Mechanics*, vol. 326, pp. 37–56, 1996.
[56] Preziosi, L., Chen, K., and Joseph, D. D., Lubricated pipelining: stability of core-annular flow, *Journal of Fluid Mechanics*, vol. 201, pp. 323, 1989.
[57] Burton, H., Section G. Deposits from whole milk in heat treatment plant—a review and discussion, *Journal of Dairy Research*, vol. 35, pp. 317–330, 1968.
[58] Lalande, M., Tissier, J.-P., and Corrieu, G., Fouling of a plate heat exchanger used in ultra-high-temperature sterilization of milk, *Journal of Dairy Research*, vol. 51, pp. 557–568, 1984.
[59] Lalande, M., and Tissier, J., Fouling of Heat Transfer Surfaces Related to beta-Lactoglobulin Denaturation During Heat Processing of Milk, *Biotechnology Progress*, vol. 1, pp. 131–139, 1985.

ISBN: 978-0-9984188-3-4; Published online www.heatexchanger-fouling.com